University of Groningen

Quantized conductance of a suspended graphene nanoconstriction

Tombros, Nikolaos; Veligura, Alina; Junesch, Juliane; Guimaraes, Marcos H. D.; Vera-Marun, Ivan J.; Jonkman, Harry; van Wees, Bart

IMPORTANT NOTE: You are advised to consult the publisher's version (publisher's PDF) if you wish to cite from it. Please check the document version below.

Document Version
Publisher's PDF, also known as Version of record

Publication date:
2011

[Link to publication in University of Groningen/UMCG research database](#)

Quantized conductance of a suspended graphene nanoconstriction

Supplementary Information

1. Current annealing

Current annealing of suspended graphene membranes was performed by ramping up the DC current across the suspended graphene devices for each measured region separately in vacuum (2.0 10^{-7} mbar) at a temperature of 4.2K. Our method is not fundamentally different from the standard one except that we push it to the limit in order to make graphene constrictions. While increasing the DC current through the devices the resistance of the device was monitored. At typical current densities of approximately 7 A/cm (about a current of 1.5 mA) the resistance starts increasing rapidly, indicating the combination of two effects: the increase in the graphene temperature (to T > 500°C), followed by the shift of the charge neutrality point from a highly doped state (usually p-doped) towards zero gate voltage. The current density required to clean the graphene membranes varies from sample to sample and depends on the length and width of the graphene. We relate this to the fact that suspended graphene cools down via the metal contacts, the closer they are the higher the current density required to bring the charge neutrality point to zero (hence reach high enough temperature for desorbing polymer remains from the graphene surface). In Fig.S1 a scanning electron microscopy (SEM) image of a typical suspended device is shown. Regions A and B are annealed with current densities of 6.8 and 4.8 A/cm respectively. For comparison the region C was left untouched and shows highly p-doped state. In the SEM picture one can see the difference between the current annealed and non-annealed regions. The region C shows a homogeneously coverage of residues, which is not observed in the annealed regions. Note also that the graphene layer has a tendency to constrict after current annealing as in region A (see also Fig.1a in the main text). In several cases the devices break during the

annealing procedure. About 20% of the 2-probe regions survive the current annealing step and become high mobility samples.
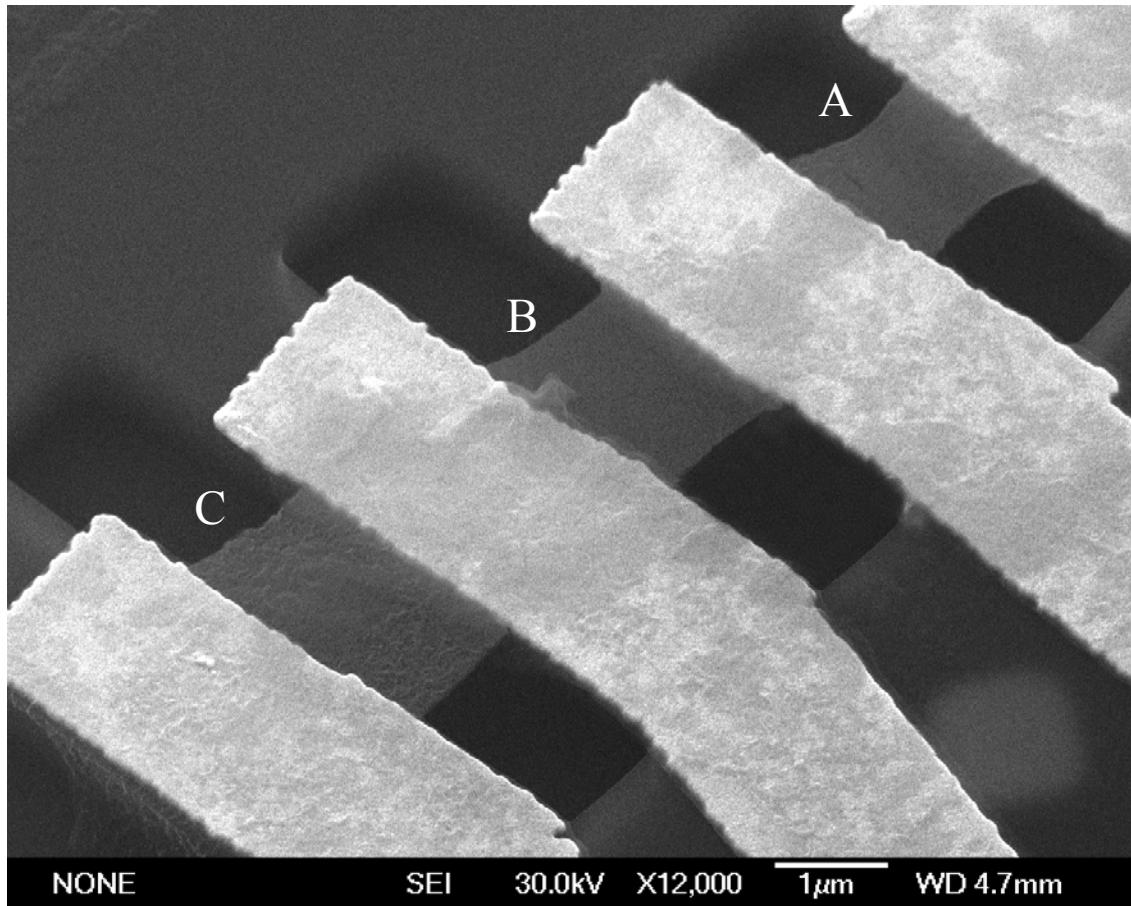

Figure S1. SEM image of a typical suspended device on LOR polymer. Regions A and B were annealed with DC current while C was left untouched for comparison.

2. Overview of measured devices

We fabricated about 20 two-probe devices with different dimensions. Here we present the results of electronic transport close to the ballistic regime for 4 different samples. In Figures S2, S3, S4 and S5 we present the resistance and conductance as a function of gate voltage V_g (a and b respectively), c) the conductance as a function of the Fermi wavenumber k_F and d) the mean free path (λ)of the charge carrier versus k_F for each sample (#1 to #4)

For each separate case the capacitance of the system (α) was determined from the filling factors in the quantum Hall regime. In the calculations we used $n = \alpha \ (V_g - V_D)$, where n is the induced charge carrier density and V_D is the position of the charge neutrality point. The Fermi wavenumber was obtained from the relation $k_F = \sqrt{\pi \ n}$. We extract the mean free path of the charge carriers using the Einstein relation for conductivity $\sigma = \nu \ e^2 D$, where ν is the density of states for a single graphene layer and the diffusion constant in two-dimensions is given by $D = \frac{1}{2}\nu_F\lambda$, with ν_F is Fermi velocity and λ the mean free path. Substituting $\nu = \frac{g_v g_s 2\pi|\varepsilon|}{h^2 v_F^2}$ and $|\varepsilon| = \mathbf{h}v_F k_F$ we obtain

$$\lambda = \frac{\sigma h}{2e^2 k_F} .$$

The length L and width W of the samples are indicated in each of the figures S2, S3, S4 and S5 in panel a). From 2-probe, 3-probe and 4-probe measurements we extract a very low contact resistance between the graphene layer and the Ti/Au electrodes, typically 50Ω per contact. For each sample we calculate the number of expected one-dimensional modes (N) through the channel $N = \frac{k_F W}{\pi}$ at a specific value of k_F and also the corresponding ballistic conductance $G_{bal} = \frac{4e^2}{h}\frac{k_F W}{\pi}$
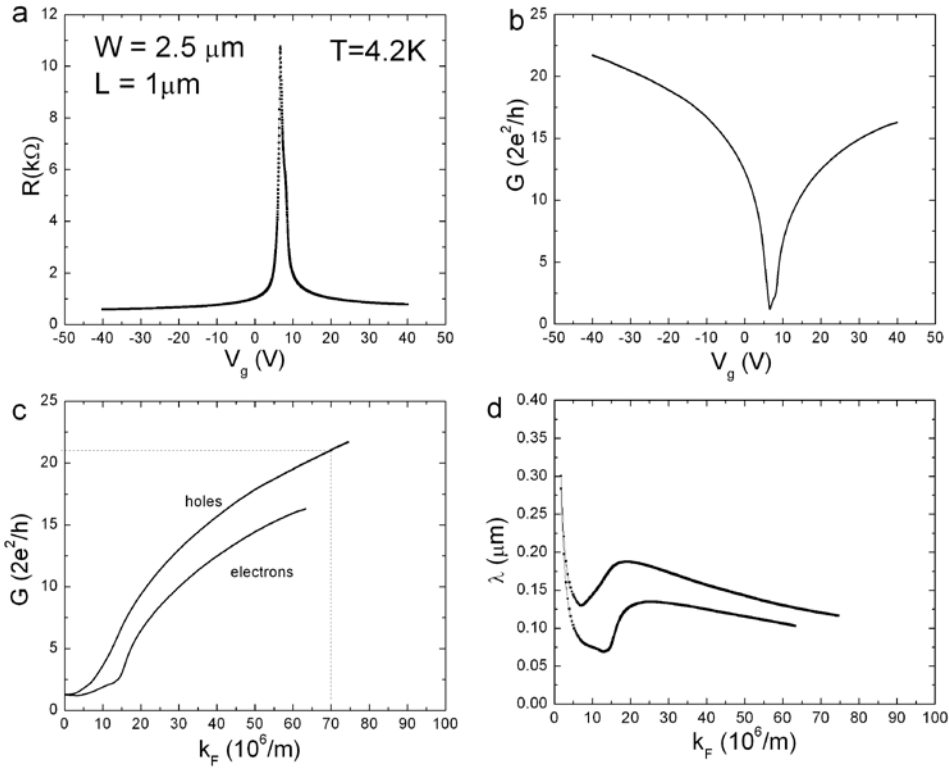
Figure S2.

For sample #1 (Fig S2) the calculated value of conductance at $k_F = 70 \times 10^6$/m according to its width (2.5 µm) is $110 \times 2e^2/h$, while the measured value was $\sim 21 \times 2e^2/h$. The transmission of the channel is around 19% which corresponds to a mean free path of 190 nm in agreement with the mean free path extracted from the Einstein relation (Fig. S2 d).
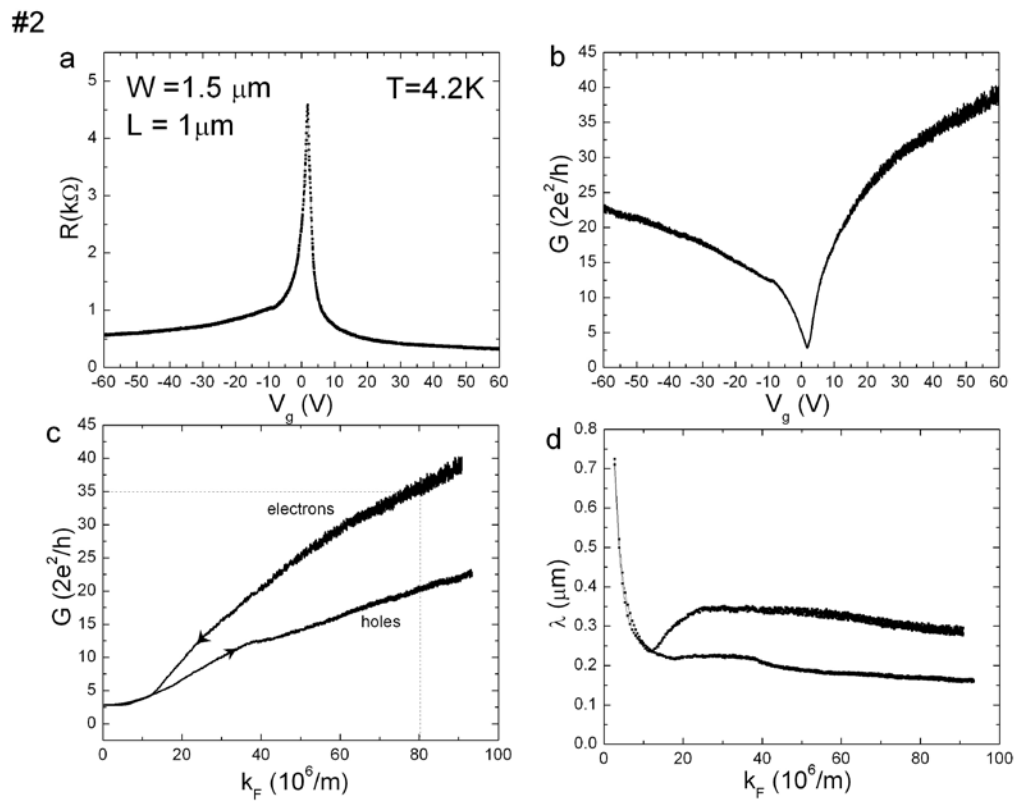
Figure S3.

The same calculations of the conductance for Sample #2 (Fig S3) at k_F = 80×10^6/m and for the width (1.5 µm) results in $G = 75 \times 2e^2$/h, while the measured value was $G \sim 35 \times 2e^2$/h, which means that the transmission of the channel is about 45% and a mean free path of 450 nm.
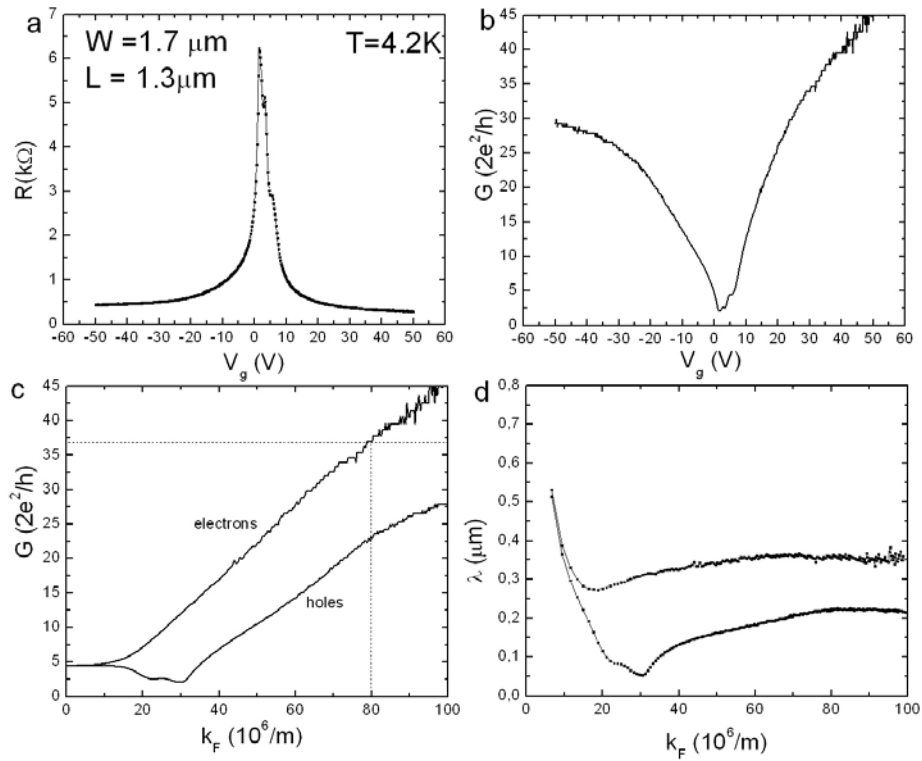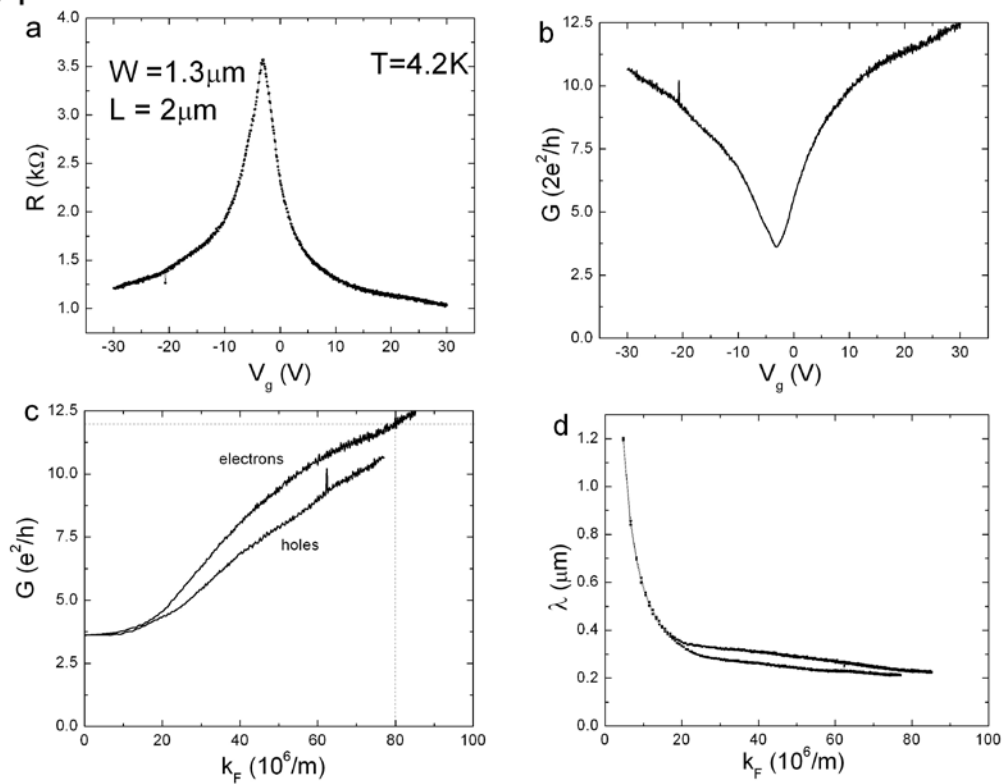
#3

Figure S4.

For Sample #3 (Fig S4) at $k_F = 80 \times 10^6$/m and for the width (1.5 µm) $G = 85 \times 2e^2$/h, while the measured value was $G \sim 37 \times 2e^2$/h, giving a transmission of 43% and a mean free path of 430 nm.

#4

Figure S5. Sample #4

According to the number of calculated modes, sample #4 (Fig. S5) has 18% transmission and a mean free path of 360 nm at $k_F = 80 \times 10^6$/m
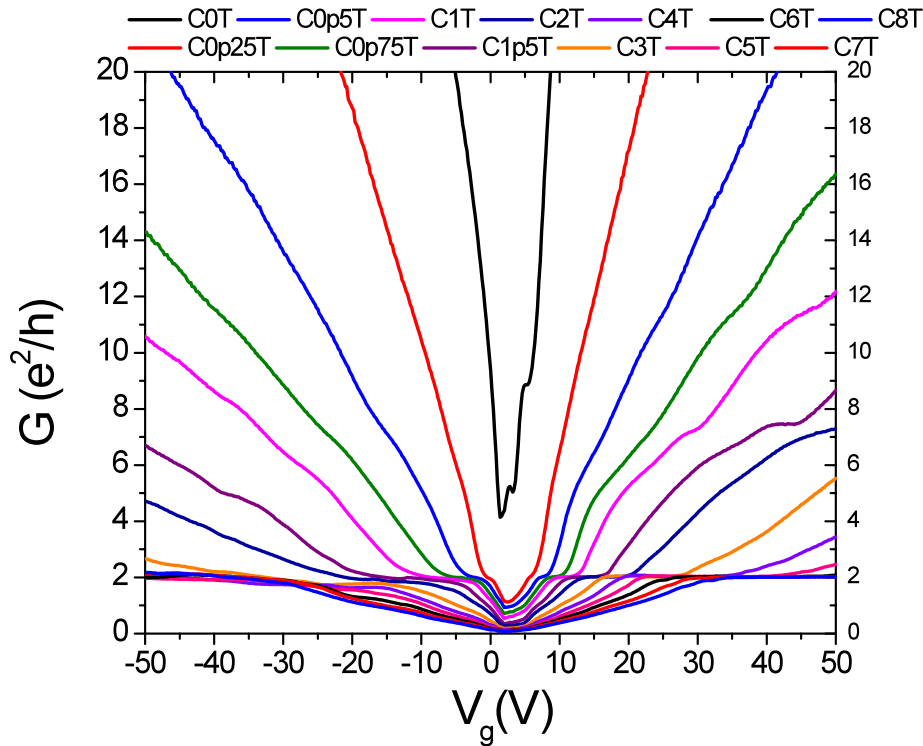
Figure S6. Observed QHE in sample #3.

In Figure S6 we show the QHE for Sample #3. The $2e^2/h$ plateau is observed down to a magnetic field of 250 mT indicating high quality graphene. However, the position of the Dirac point at 2.5V and the non-well developed plateaus at 6, 10 and 14 e^2/h indicate some inhomogeneity in the residual doping. Note that in this sample the $2e^2/h$ plateau does not extend down to 0T in contrast to the sample discussed in the main text.

Table 1 Dimensions and maximum resistance R_{max} for different samples

Sample name	Dimensions, µm	R_{max} (kΩ) after annealing
Sample showing quantized conductance for both electrons and holes (see main manuscript)	L=1 W=2.5 before annealing W= 0.3 after annealing	21.7
Sample #1	W=2.5; L=1	10.5
Sample #2	W=1.5; L=1	4.5
Sample #3	W=1.7; L=1.3	6.2
Sample #4	W=1.3; L=2	3.5

In table 1 we show the resistance R_{max} at the charge neutrality point after the annealing step. The highest resistance was obtained for the sample presented in the manuscript which showed quantized conductance as a result of formation of a constriction. We note that the position of the Dirac point for the device presented in the manuscript is found at 0.8V. This is much closer to 0V as compared to the devices #1-#4 and this points to the fact that there is a very small inhomogeneity due to residual doping.

In conclusion, the devices fabricated with the current annealing step show a mean free path of several hundred nanometers at high charge carrier density and even longer at lower density. The device described in the main text has the best transport properties of all investigated devices.

3. Magnetic field offset

We can exclude that the conductance quantization we measured at zero magnetic field B is a result of any remaining magnetization of the superconducting magnet for the following reasons:

1) The conductance quantization does not disappear when we scan the range -100mT to 100mT. From the symmetry between +B and –B we conclude that any remaining magnetization from the superconducting magnet (or other sources) is less than 1mT.

2) The conductance quantization at 4.2K persists when the sample is positioned 20 cm above the superconducting magnet (set to zero field).

3) At a temperature of approximately 12 K, at which the magnet is not in the superconducting state anymore, we still measure quantized conductance.